Title: The $P2Y_{13}$ receptor regulates phosphate metabolism and FGF-23 secretion with effects on skeletal development.

Ning Wang[a], Bernard Robaye[b], Fatima Gossiel[a], Jean-Marie Boeynaems[b,c], Alison Gartland[a1]

[a]The Mellanby Centre for Bone Research**,** Department of Human Metabolism, The University of Sheffield, Sheffield, UK, [b]Institute of Interdiscipinary Research, IRIBHM, Université Libre de Bruxelles, Gosselies, Belgium, [c] Department of Medical Chemistry, Erasme Hospital, Brussels, Belgium

1 Corresponding author and person to whom reprint requests should be addressed:

Dr Alison Gartland,

The Mellanby Centre for Bone Research

Department of Human Metabolism

The University of Sheffield

Beech Hill Road

Sheffield, S10 2RX

UK

Phone: (+44) 0114 226 1435

Fax: (+44) 0114 271 1711

Email: a.gartland@sheffield.ac.uk

Short title: P2Y13 receptor KO mice and phosphate metabolism

Abbreviation list.

3D: three dimentional

ALP: alkaline phosphatase,

ADP: adenosine diphosphate

ATP: adenosine triphosphate

BMD: bone mineral density

BV: bone volume

BV/TV: bone volume fraction

CKD-MBD: chronic kidney disease mineral bone disorder

CT: threshold cycle

DA: degree of anisotropy

FGF-23: fibroblast growth factor 23

H&E: hematoxylin and eosin

KO: knock-out

NaPi-II: type II Na+-dependent inorganic phosphate cotransporter

N.Ob/B.Pm: osteoblast number/bone perimeter

N.Oc/B.Pm: Osteoclast number/bone perimeter

Ob.Pm/B.Pm: the proportion of bone surface occupied by osteoblasts

Oc.Pm/B.Pm: the percentage of bone surface occupied by osteoclasts

PTH: parathyroid hormone

SMI: structure model index

Tb.N: trabecular number

Tb.Pf: trabecular pattern factor

Tb.Th: trabecular thickness

TRAP: tartrate resistant acid phosphatase

TV: tissue volume

μCT: micro-computer tomography

WT: wild type

Abstract:

Purinergic signalling mediates many cellular processes including embryonic development and regulation of endocrine signalling. The ADP $P2Y_{13}$ receptor is known to regulate bone and stem cells activities, although relatively little is known about its role in bone development. In this study we demonstrate, using contemporary techniques that deletion of the $P2Y_{13}$ receptor results in an age-dependent skeletal phenotype that is governed by changes in phosphate metabolism and hormone levels. Neonatal and postnatal (2 weeks) $P2Y_{13}$ receptor knock-out mice (KO) were indistinguishable from their wild type littermate controls (WT). A clear bone phenotype was observed in young (4-week old) KO mice compared WT controls, with 14% more trabecular bone, 35% more osteoblasts, 73% less osteoclasts and a 17% thicker growth plate. Mature (>10 weeks of age) KO mice showed the opposite bone phenotype with 14% less trabecular bone, 22% less osteoblasts and 10% thinner growth plate. This age dependent phenotype correlated with serum fibroblast growth factor-23 (FGF-23) and phosphorus levels which were 65% and 16% higher respectively in young KO mice but remained unchanged in mature mice. These findings provided novel insights for the role of the $P2Y_{13}$ receptor in skeletal development via coordination with hormonal regulators of phosphate homeostasis.

Key words: $P2Y_{13}$ receptor, knock-out, bone phenotype, phosphate metabolism, FGF-23

Introduction

Purinergic signalling plays important roles in many pivotal events of biological process, such as neurotransmission, cell growth, proliferation, and death (1). The expression and function of purinergic receptors occur throughout embryologic development and have been studied in a wide variety of organisms and in many organs, including the heart, eye, skeletal muscle and the nervous system (2). Several studies link purinergic signalling with the development of skeletal system, mostly based on the involvement of purinergic receptors and their agonists in chondrocyte proliferation, maturation and matrix mineralization and hence endochondral ossification (3-8). However, whether purinergic receptors regulate skeletal development via an endocrine or paracrine manner is still unknown.

The $P2Y_{13}$ receptor, a member of the P2Y receptor subfamily and originally discovered in 2001, is a G_i-coupled receptor with high affinity for ADP (9-11). The $P2Y_{13}$ receptor was widely detected in different tissues especially in the brain and pituitary of both human and rodents (9, 12, 13) and was shown to be involved in various biological processes especially in the neurological field (14-18). The $P2Y_{13}$ receptor was also shown to affect osteoblast and osteoclast activities directly (19) and regulate the differentiation direction towards osteoblast from mesenchymal stem cell (20), providing evidences that it may play a role in endochondral ossification directly via regulating differentiation/function/proliferation of bone cells. Furthermore, our recent findings demonstrated that depletion of $P2Y_{13}$ receptor can change the alkaline phosphatase (ALP) activity of osteoblasts and alter the extracellular ATP concentration in response to mechanical stimuli (21) indicating the involvement of $P2Y_{13}$ receptor in phosphate metabolism. Importantly, the alteration of serum phosphate levels in both human and rodents has been shown to cause changes in the primary phosphate homeostasis regulator fibroblast growth factor 23 (FGF23) (22-24). These changes were mainly caused by osteoblasts/osteocytes and result in skeletal development defects in both human and rodents (25-28). These data indicate that the $P2Y_{13}$ receptor may mediate skeleton development and bone modelling in an endocrine manner via hormones such as FGF23.

To test this hypothesis, we used $P2Y_{13}$ receptor knock-out (KO) mice as model and performed whole mount alizarin red/alcian blue staining and Micro-CT (μCT) analysis on neonatal mice to investigate the early skeletal development. Bone phenotype alteration was also determined at different ages: pre-puberty (2 weeks), puberty (4 weeks), mature (10

weeks) and cessation of longitudinal growth (16 weeks) using μCT and histomorphometry analysis. To investigate the mechanism, serum ALP, phosphorus, calcium, and FGF23 level were measured. The expression of the Fgf23 gene in samples from both mouse bone marrow and osteoblast was determined.

Materials and Methods

Mice

The KO mouse was generated on the C57BL/6J background as previously described (18). KO and WT littermate controls were housed in the same environmentally controlled conditions with a 12hr light/dark cycle at 22°C, with free access to 2018 Teklad Global 18% Protein Rodent Diet containing 1.01% Calcium (Harlan Laboratories, Derby, UK) and water ad libitum in sterile RB-3 cages. Mice were euthanized at neonatal (less than 24 hours), 2 weeks, 4 weeks, 10 weeks, and 16 weeks of age. Hind limbs were dissected free of attached soft tissue for bone phenotype investigation. The lengths of tibiae and tail were measured ex vivo using calibrated vernier callipers. All procedures complied with the UK Animals (Scientific Procedures) Act 1986 and were reviewed and approved by the local Research Ethics Committee of the University of Sheffield (Sheffield, UK).

Whole mount neonatal mice skeletal staining

Neonatal littermate mice (less than 24 hrs old) were skinned, eviscerated, and fixed in 90% ethanol and dehydrated for at least 7 days. The samples were stained at room temperature in 0.1mg/mL Alcian Blue 8GX solution (Sigma-Aldrich Ltd, Poole, Dorset, UK) in ethanol with 20% glacial acetic acid for 3 days and then rehydrated through a graded series of ethanol (2 ~ 3 hrs rehydration in the concentration of 70%, 40%, 15% and dH_2O). The samples were placed in freshly prepared 1% KOH solution for two days until soft tissue was translucent, followed staining in alizarin red solution (0.025M in 1% KOH) for 3 days and immersed in 1% KOH solution for 3 times (2 ~ 3 hrs each time). The stained samples were then passed through a graded series of glycerol (20%, 50% and 70% for 24 hrs each) and stored in 100% glycerol. General skeletal development morphology was examined under a Technico dissecting scope. Right femur length, mid shaft diameter, and ossification bone length were all quantified using calibrated vernier callipers to address whether $P2Y_{13}$ receptor deficiency led to alteration in endochondral ossification.

μCT

The high-resolution SkyScan 1172 scanner (SkyScan, Kontich, Belgium) was used to investigate the phenotype of bone micro-architecture. The X-ray source was operated at 50kV and 200μA with a 0.5 mm aluminium filter. For whole neonatal mice skeleton, the whole bodies were two-parts oversize scanned at the resolution of 17.2μm and the region of interest (ROI) was then selected to include all the tissues and then analyzed using Skyscan CTan software (SkyScan, Kontich, Belgium). The parameters mainly included the bone volume fraction (BV/TV), bone volume (BV), tissue volume (TV), and bone mineral density (BMD). For the long bone μCT analysis, right tibiae were dissected free of soft tissue, fixed in 70% ethanol, and then scanned at the resolution of 4.3μm. Different ROIs were selected according to age of the mice. Tibia proximal end trabecular morphometry of mature mice (above 10 weeks of age) was characterized by measuring structural parameters from a 1.0mm thick trabecular abundant region which was 0.2mm lower than the growth plate (19). For 2 and 4 weeks old mice, tibial trabecular was measured from a 0.5mm thick region which was 0.5mm and 0.7mm below the top edge of growth plate respectively. The trabecular bone related quantitative parameters measured included BV/TV, trabecular thickness (Tb.Th), trabecular number (Tb.N), trabecular pattern factor (Tb.Pf), structure model index (SMI), degree of anisotropy (DA), and BMD. BMD was expressed as gram of hydroxylapatite per cube centimetre as shown before (19). Three-dimensional (3D) models were also built to determine any morphological changes.

Bone histomorphometry

The left tibiae were fixed in 10% buffered formalin and decalcified in 14.3% EDTA for 4 weeks. After embedded in paraffin wax, the samples were cut into sections by a Leica Microsystems Microtome at 3 μm in depth. The sections were then Tartrate resistant acid phosphatise (TRAP) stained as described previously, using Naphthol AS-BI phosphate (Sigma-Aldrich Ltd, Poole, Dorset, UK) as an initial substrate for TRAP (19). The number of osteoblasts (N.Ob/B.Pm), the proportion of surface occupied by osteoblasts (Ob.Pm/B.Pm), the number of osteoclast (N.Oc/B.Pm), and the percentage of surface occupied by osteoclasts (Oc.Pm/B.Pm) were determined on a 3 mm length of endocortical surface, starting 0.25mm from the growth plate viewed on a light DMRB microscope (Leica Microsystems, Wetzlar, Germany). The sections were also stained with Gill's II haematoxylin (VWR international Inc, Lutterworth, Leicestershire, UK) and 1% aqueous eosin (VWR international Inc,

Lutterworth, Leicestershire, UK) (H&E) to measure the average widths of growth plate and the width of proliferation zone using a light DMRB microscope. All histomorphometric parameters were based on the report of the ASBMR Histomorphometry nomenclature (29) and were obtained using the Osteomeasure bone histomorphometry software (Osteometrics, Decatur, GA, USA).

TaqMan assay

The expression alterations of Fgf23 was evaluated with a TaqMan assay using total RNA from primary osteoblasts isolated from neonatal mouse calvarias and long bone marrow isolated from 9 weeks old mice, as described previously (19). Briefly, the total RNA was extracted with TRI Reagent (Sigma-Aldrich Ltd, Poole, Dorset, UK) and the cDNA was synthesized using Promega ImProm-II™ reverse trancriptase (Promega, Southampton, UK) with Oligo(dT) 15 primer (Promega, Southampton, UK) according to manufacturer's instruction. The quantitative RT-PCR amplification of the TaqMan assay was then performed on an Applied Biosystems 7900HT Real-Time PCR system (Life Technologies Ltd, Paisley, UK) with thermal cycling conditions: 2 mins at 50°C, 10 mins at 94.5°C, followed by 40 cycles of denaturation at 97°C for 30 sec and extension at 59.7°C for 1 min (30). The fold changes of Fgf23 expression comparing between KO and WT was analysed using the Applied Biosystems SDS 2.2.1 software (Life Technologies Ltd, Paisley, UK) based on the threshold cycle (CT) relative quantification method (31). Briefly, the quantification of Fgf23 cDNA was firstly normalized to the endogenous control gene: β-actin (Actb) and ΔCT calculated ($\Delta CT = CT_{Fgf23} - CT_{Actb}$). The difference in expression between the WT and KO mice was then expressed as ΔΔCT ($\Delta\Delta CT = \Delta CT_{WT} - \Delta CT_{KO}$). Fold changes of expression were finally calculated by taking 2 to the power of the ΔΔCT ($2^{\Delta\Delta CT}$).

Serum Biochemical Markers Analysis

Blood samples were collected from KO and age matched WT control mice (4 weeks for young mice, 16-20 weeks for mature mice, $n \geq 3$) via intracardiac puncture under deep non-recovery anaesthesia. Blood samples were then left to clot at room temperature and concentrated at 4,000rpm for 10 mins. The top aqueous phase (serum) was isolated and stored for further analysis. The serum Calcium, Phosphorus, and ALP were determined with colorimetric methods (cresolphtalein, phosphomolybdate, and p-nitrophenyl phosphate

respectively) on Modular Analytics analyser (Roche Diagnostics, Basel, Switzerland). 25-0H vitamin D3 was measured using an immunometric method with chemoluminescence on Liaison (Diasorin, Saluggia, Italy). FGF-23 ELISA kit (Kainos Laboratories Inc., Tokyo, Japan) was used to measure the circulating FGF-23 levels. All procedures were performed according to manufacturer's instructions.

Statistic analysis

All data are expressed as mean ± SEM. Statistical significance was tested for using an unpaired t-test with Prism 5 software (GraphPad, La Jolla, CA, USA).

Results

Gross bone phenotype of neonatal KO mice

Littermates pups obtained from heterozygous breeding pairs were euthanized and genotyped within 24 hours after birth. No obvious gross difference was observed and there was no significant difference in body weight between KO and WT littermates (Figure 1A + B). KO and WT littermate controls were then μCT scanned and three-dimensional (3D) skeletal models were constructed. Visual analysis of the 3D models revealed no morphological abnormalities in the skeleton of KO mice (Figure 1C), with quantification of the scan data confirming no significant differences between KO and WT littermate controls (Figure 1D).

Neonatal endochondral ossification in KO mice

To address whether $P2Y_{13}$ receptor deletion will lead to abnormal embryonic skeletal development, especially in the endochondral ossification process, the neonatal pups were skinned, eviscerated, and stained with alizarin red/alcian blue. After staining, the cartilage and ossified bone was clearly stained as blue colour by alcian blue and red colour by alizarin red respectively. All of the ossification centres in the vertebral bodies of the trunk in both KO and WT were present, as is expected at birth. In the coccyx, only coccygeal 1 to 5 had ossified in the majority of both KO and WT mice (Figure 1E). The whole length, mid shaft diameter, and ossification bone length of right femurs were measured as shown in Figure 1F using a calibrated vernier calliper, to address whether $P2Y_{13}$ receptor deficiency leads to alteration in endochondral ossification. No significant differences between KO and WT were found in the whole femur length (3.89 ± 0.11 mm versus 3.89 ± 0.10 mm, $p = 0.9740$, Figure 1G), the percentage of ossified bone to whole femur length (53.5 ± 1.3 % versus 52.9 ± 1.8 %,

p = 0.7780, Figure 1H), or the mid shaft diameter (0.82 ± 0.02 mm versus 0.78 ± 0.03 mm, p = 0.3044, Figure 1I).

Changes in tibia trabecular parameters with age in KO mice

Analysis of the trabecular bone structure of the tibial region was performed using μCT analysis. The trabecular bone mass increase and architecture changes with age can be clearly distinguished in images from the 3D models of the tibial trabecular bone in different aged mice (Figure 2A). Quantitative μCT data showed both WT and KO mice reached peak mass (BV/TV) at the age of 10 weeks. In WT mice, peak BV/TV plateaued until 16 weeks, however, in KO mice a drastic decrease in BV/TV (31.4%, p = 0.0035) occurred after peak bone mass. In terms of relative bone volume, there was no significant differences at 2 weeks of age, however KO mice had significantly higher BV/TV at 4 weeks of age (13.5%, p = 0.0326) but significantly lower BV/TV at 10 weeks (14.4%, p = 0.0170) and 16 weeks of age [37.5%, p < 0.001(19)] (Figure 2B). A similar trend was found in trabecular number (Tb.N), where KO showed slightly increased Tb. N at 4 weeks of age (6.5%, p = 0.284) but significantly lower Tb. N at 10 weeks (21.8%, p = 0.0027) and 16 weeks of age [37.8%, p < 0.0002 (19)] (Figure 2C). All the quantitative μCT data are summarized in Table 1.

Changes in bone cells in KO mice

Cobblestone like osteoblasts and TRAP positive osteoclasts were easily identified and quantified on the tibia endocortical surface (Figure 3A, 3B). At 4 weeks of age, KO mice showed 35% more osteoblasts per mm bone (N.Ob/B.Pm, 71.15 ± 3.61 versus 52.89 ± 5.61, p = 0.0209) and 33% higher bone surface occupied by osteoblasts (Ob.Pm/B.Pm, 0.87 ± 0.02 versus 0.65 ± 0.04, p = 0.0005) than WT (Figure 3C, 3D). However, the N.Ob/B.Pm and Ob.Pm/B.Pm were both significantly lower in KO mice than in WT mice at 16 weeks of age (19). In terms of osteoclasts, KO mice had a significant reduction in both the number of osteoclast per mm bone surface (N.Oc/B.Pm, 73% less, 1.11 ± 0.22 versus 4.17 ± 0.52, p = 0.0003) and the percentage of bone surface occupied by osteoclasts (Oc.Pm/B.Pm, 70% less, 0.03 ± 0.01 versus 0.10 ± 0.01, p = 0.0001) compared to WT at 4 weeks of age (Figure 3E, 7.3F). The same reduction in N.Oc/B.Pm and Oc.Pm/B.Pm compared to WT was also found in mature mice at the age of 16 weeks (19).

Osteoblasts and osteoclasts were also identified and quantified in a trabecular bone abundant region of the tibia, with a similar trend being detected. At 4 weeks of age, KO mice had 41% higher N.Ob/B.Pm (42.38 ± 9.14 versus 30.00 ± 4.13, p = 0.2456) and 35% higher Ob.Pm/B.Pm (0.40 ± 0.09 versus 0.29 ± 0.03, p = 0.3126) than WT on trabecular bone. KO mice also demonstrated reduction in N.Oc/B.Pm (9.45 ± 0.68 versus 11.02 ± 0.64, p = 0.1214) and Oc.Pm/B.Pm (0.22 ± 0.02 versus 0.27 ± 0.02, p = 0.1303) compared to WT on trabecular bone. In 16 weeks old mice, the N.Ob/B.Pm and Ob.Pm/B.Pm were both significantly lower in KO mice than WT mice. However, there were no significant differences between KO and WT mice in N.Oc/B.Pm and Oc.Pm/B.Pm (19).

Bone length changes with age in KO mice

To examine the effects of $P2Y_{13}$ receptor depletion on bone growth, the lengths of the tibia and tail [as indicators of growth rate (32)] at different ages (2 weeks, 4 weeks, 10 weeks, and 16 weeks of age) were measured using calibrated vernier callipers. As expected both the tibial and tail length of WT and KO mice increased with age. At 10 weeks of age, the tibial length of the KO mice was 4% longer (17.12 ± 0.04 mm versus 16.54 ± 0.07 mm, $p < 0.0001$) than that of WT. This difference in length was lost by 16 weeks (Figure 4A). The tails of the KO mice were significantly longer than WT at 4 weeks (4% longer, 65.52 ± 0.69 mm versus 62.78 ± 0.42 mm, p = 0.0068) and 10 weeks (7% longer, 81.64 ± 0.63 mm versus 76.43 ± 0.46 mm, $p < 0.0001$). Again, this difference was lost by 16-weeks (Figure 4B).

Alterations in the structure of the growth plate in KO mice with age.

To determine whether $P2Y_{13}$ receptor deficiency could influence chondrocyte proliferation and differentiation and hence endochondral ossification, the total width (excluding ossification zone) and the width of the proliferation zone of the proximal end growth plates at different ages were measured on the tibial H&E staining sections. Both KO and WT mice showed growth plate narrowing with aging. Compared to WT mice, KO mice growth plate showed a less organized pattern, especially in the proliferation zone (Figure 4C). At 4 weeks of age, KO mice had 17% thicker total growth plate (254.5 ± 3.1 μm versus 218.1 ± 5.2 μm, p = 0.0001) and 18% wider proliferation zone (115.0 ± 4.8 μm versus 97.1 ± 5.3 μm, p = 0.0321). However at 10 weeks of age, KO mice had significantly reduced growth plate width (10%, 105.2 ± 2.9 μm versus 117.0 ± 2.9 μm, p = 0.0118) and a thinner proliferation zone (17%, 56.5 ± 1.0 μm versus 68.3 ± 1.0 μm, $p < 0.0001$). The reduction in growth plate (13%, 106.3 ± 2.8 μm versus 122.2 ± 2.0 μm, p = 0.0009) and proliferation zone widths (12%, 62.0

± 1.4 μm versus 70.4 ± 1.1 μm, p = 0.0008) (Figure 4D, 4E) were also apparent in 16 weeks old KO mice.

Changes in serum biochemical markers

Serum markers were examined to elucidate the systemic changes relevant to skeletal development abnormity. Four week old KO mice showed a significant 16% increase in serum phosphorus levels (9.06 ± 0.20 mg/dL versus 7.84 ± 0.50 mg/dL, p = 0.0497) (Figure 5A) but no significant difference in serum calcium levels (9.16 ± 0.07 mg/dL versus 9.05 ± 0.15 mg/dL, p = 0.5347) (Figure 5B), compared to age matched WT controls. The serum FGF23 level of KO was 65% higher than that of WT (111.0 ± 11.8 pg/mL versus 67.3 ± 10.5 pg/mL, p = 0.0241) (Figure 5C), while there were significant decreases in the KO serum ALP level (31%, 276.6 ± 21.7 UI/L versus 402.3 ± 10.4 UI/L, p = 0.0001) and 25-OH vitamin D3 level (24%, 56.0 ± 1.7 ng/mL versus 74.0 ± 4.6 ng/mL, p = 0.0232) (Figure 5D, 5E). However, there were no significant differences in any of these markers between WT and KO mature mice above 16 weeks of age.

Fgf23 gene expression in KO mice

To delineate the change in FGF-23 expression alteration after the deletion of P2ry13 gene, a TaqMan array and real-time PCR were used to analyse Fgf23 gene expression in cDNA from primary osteoblasts isolated from neonatal mouse calvaria and long bone marrow isolated from 9 weeks old WT and KO mice with threshold cycle (CT) relative quantification method (33). KO mice showed significantly increased Fgf23 expression compared to WT control (6.5 and 7.3 folds higher respectively in primary osteoblast and bone marrow samples).

Discussion

We have previously shown that the $P2Y_{13}$ receptor directly regulates bone turnover in mature female mice (19) and there is also evidence that the $P2Y_{13}$ receptor can potentially interact with systemic hormones. Given these observations and the known role of purinergic signalling in development (3-8), we postulated that the $P2Y_{13}$ receptor may play a potential role in skeletal development. Therefore in this study, we investigated the bone morphology of different aged KO mice and demonstrated an age dependent bone phenotype.

The gross phenotype including body weight and the whole skeleton investigation using μCT analysis showed that there were no significant differences between neonatal KO and WT mice littermates in any of the parameters measured. This was confirmed by the results from whole mount alizarin red/alcian blue staining where there were no length or diameter alterations in the ossified bone or cartilage of the long bone. These data indicated that deletion of $P2Y_{13}$ receptor did not affect the mice skeletal development especially the endochondral ossification at embryonic or neonatal stage.

However, the trabecular bone data obtained using μCT demonstrated a clear age dependent phenotype. At 2 weeks of age, KO mice showed no significant differences in the majority of the trabecular bone parameters compared to WT mice, with the exception of significantly thicker trabecular. When KO mice reach 4 weeks old, which overlaps with puberty of C57BL/6J female mice (34), there was a significant increase in trabecular bone volume (BV/TV). This increase in trabecular bone of KO mice only existed for a short period of time and diminished quickly. By the time the mice had reached maturity (between 10 and 16 weeks) the trabecular bone volume had become significantly less than WT. As previously described (19), this significant reduction in trabecular bone was a result of decreased trabecular number and architecture changes (from plate like to rod like), rather than any trabecular thickness alterations. Therefore, there was a clear trabecular phenotype switch with aging in KO mice from more trabecular bone at about puberty age but less trabecular in mature mice compared to WT. This phenotype switch was further confirmed and also explained by the histomorphometry results. The 4 weeks old KO mice had more osteoblasts compared to WT, while there were significantly less osteoblasts on both trabecular and cortical bone surface in 16 weeks old KO mice. On the contrary, the alteration patterns of osteoclasts at the two age point were the same with reduced osteoclast number at both ages, especially significant on the endocortical surface. Therefore, the bone phenotype changes were mainly due to the changes of osteoblasts instead of osteoclasts.

The higher endocortical osteoblastic parameters in 4 weeks old KO mice might indicate greater bone length rather than cross-sectional changes. This was confirmed with the measurements of tibia and tail length which are easily obtained parameters for mice growth rate (35). Both 4 and 10 weeks old KO mice showed significantly longer tails, whilst the length of the tibia was longer in KO mice by 10 weeks of age. This could be due to the

longitudinal long bone growth spurts that occur after onset of puberty (36) and that tibial bone length differences could only be detected in older KO mice such as 10 weeks old mice. The growth plate is the main organ for longitudinal growth via chondrocyte proliferation and differentiation (36). From the measurements of the growth plates at different age points, 4 weeks old KO mice showed wider growth plate than WT mice especially in the proliferation zone; the wider growth plate would lead to the longer bone phenotype detected at 10 weeks.

To elucidate whether the mechanism behind this age dependent bone phenotype involves phosphate metabolism and FGF23 function changes, the gene expression of Fgf23 was compared between KO and WT in mRNA samples isolated from osteoblast and bone marrow. Serum markers, including phosphorus, calcium, ALP, FGF23, and 25-OH vitamin D3, were also examined and compared between age matched KO and WT controls. Up-regulation of Fgf23 expression was found in KO mice osteoblast and bone marrow RNA samples, which was confirmed at protein level where serum FGF23 level of 4 weeks old KO was 65% higher compared to WT controls. However, FGF23 levels showed no significant differences between KO and WT when mice reached a mature age. Hence, it is clear that the age dependent bone phenotype change is correlated with these alterations of FGF23. In young KO mice increased FGF23 levels correlates with increased osteoblast number and trabecular bone mass, increase bone mineral density (Table 1), expanded growth plate, and longer bones. These changes could be due to the direct effect of the increased FGF23 production on the skeletal system. Previous research has demonstrated that FGF23 can affect skeletal development of mice only after 2 weeks of age (26, 37, 38), which can explain why there was no bone phenotype difference between KO and WT from neonatal to 2 weeks old. Increased FGF23 also proved to stimulate osteoblastic proliferation but inhibit mineralization (39, 40), which would explain the significantly higher number of osteoblast observed on the endocortical bone surface but reduced serum ALP level. However, the increased trabecular bone mass seems contrary to the hypo-mineralization phenotype demonstrated by Mackenzie et al in their FGF23 elevated Enpp1$^{-/-}$ model (27). This could be the result of higher serum phosphate detected in the KO mice, meaning that osteoblasts could still fulfil their mineralization, although functionally depressed (41). The expanded growth plate may also be due to overproduction of FGF23 which can widen the growth plate in rodents (42) and may involve other systemic hormone such as PTH and vitamin D (37, 43, 44). Indeed, the elevated FGF23 level correlated to a 24% decline in serum 25-OH vitamin D3 level, as expected, and may contribute to the widening of the growth plate especially the proliferation zone since

vitamin D has been shown to cause a decrease in proliferation of chondrocytes and deficiency of vitamin D leads to an enlarged growth plate (45). This biochemical marker variation including hyperphosphametia, higher FGF23, lower vitamin D and ALP levels in young KO mice is reminiscent of the chronic kidney disease mineral bone disorder (CKD-MBD) seen in both humans and a mouse model (46). However, the enhanced bone mass in young KO mice is contrary to bone mineralization deficiency characterized by CKD-MBD (47). Therefore, finding the exact mechanism behind this phenotype could provide a novel way to treat CKD-MBD.

In contrast to the changes at a young age, when the KO mice reach mature age, the serum level of phosphate, FGF23 and vitamin D showed no differences compared to age matched WT. It is also interesting to note that the KO mice showed narrower and more disorganized growth plate at mature age. This could be a result of down regulation of RhoA/ROCK signalling after $P2Y_{13}$ receptor depletion, which could decrease chondrocyte proliferation; previous studies have shown that RhoA/ROCK signalling positively correlates with chondrocyte proliferation but suppresses the hypertrophic differentiation of chondrocytes in the growth plate (48).

The molecular mechanism behind the age dependent bone phenotype changes could be that the variation of serum phosphate and FGF23 production provides a compensatory mechanism after global deletion of the $P2Y_{13}$ receptor. In young mice, elevated serum phosphate levels caused increased secretion of FGF23, as suggested by previous studies (22, 49), which in turn enhanced osteoblast proliferation. This would enable the direct negative effects of $P2Y_{13}$ receptor depletion on bone cells (19) to be overcome and would lead to a high bone mass phenotype. The reversal of the phenotype in mature KO mice, when both serum phosphate and FGF23 level return to normal, is most likely due to the direct result of $P2Y_{13}$ receptor depletion on bone cells being the predominant effect resulting in decreased bone mass of KO at this age as suggested in Wang et al., 2012 (19). The age dependent variation of serum phosphate and FGF23 production can then in turn affect other systemic hormones such as the negative regulation of vitamin D synthesis (25). This would cause a lower vitamin D level in young mice but a normal level in mature KO mice. The mechanism leading to age-related serum phosphate changes could be via a direct crosstalk between FGF23 and $P2Y_{13}$ receptor as they are both up-stream of MAPK signalling (19, 50). However, a potential involvement of the $P2Y_{13}$ receptor in phosphate renal reabsorption may also responsible, as previous reports

have demonstrated expression of the $P2Y_{13}$ receptor in both human and mouse kidney (12). $P2Y_{13}$ receptor may regulate the phosphate reabsorption via two possible mechanisms. The first mechanism is possibly due to the direct molecular link between the $P2Y_{13}$ receptor and the sodium-phosphate co-transporters NaPi-II. The $P2Y_{13}$ receptor is upstream of MAPK (ERK1) kinase pathway while activation of ERK1/2 kinase can down-regulate the NaPi-II (19, 51). Therefore, globally deleting the $P2Y_{13}$ receptor may lead to increased NaPi-II levels and hence increase phosphate reabsorption. Interestingly, NaPi-IIc expression was found to be highest in weaning mice but decrease once fully weaned (52). This could explain why the young KO mice have higher serum phosphate level but mature KO mice have normal serum phosphate. The second potential mechanism is that the $P2Y_{13}$ receptor negatively regulates ATP release and hence indirectly affects the phosphate reabsorption via other purinergic receptors. Extracellular ATP was found to be released across both apical and basolateral membranes from nearly all renal cells (i.e. nerve terminals, renal endothelial and epithelial cells) and to control renal tubular transport via various subtypes of P2 receptors (53-57). Various P2 receptors subtypes ($P2Y_1$, Y_2, Y_4, Y_6, P2X4, and P2X6) were identified in the proximal tubules where approximately 80% of phosphate reabsorption occurs, indicating the involvement of purinergic signalling in phosphate reabsorption (55, 58). The $P2Y_2$ receptor, an ATP/UTP receptor, was found to regulate the expression of the proximal tubule sodium-phosphate co-transporter NaPi-II in mice (54). Interestingly, the $P2Y_{13}$ receptor was shown to provide a negative feedback to ATP release in different cell types including red blood cells and osteoblasts (21, 59). Should this negative feedback pathway be a ubiquitous mechanism and occur in the proximal tubule, then deletion of $P2Y_{13}$ receptor may lead to increased extracellular ATP and hence affect phosphate reabsorption, coordinating with other P2 receptors in an age dependent manner. However, although the involvement of purinergic signalling in the regulation of renal transport has becoming an expanding field in the past decade, the exact roles of P2 receptors in renal phosphate reabsorption is unclear. Clearly, further investigation on the role of $P2Y_{13}$ receptor in this process, especially in ATP regulated phosphate reabsorption, is required and beyond the scope of this current study.

In conclusion, the age dependent bone phenotype caused by the global deletion of the $P2Y_{13}$ receptor provides evidence that the $P2Y_{13}$ receptor plays an important role in moderating skeletal development via two distinct manners. One is the endocrinal regulation of phosphate and FGF23 homeostasis and predominantly happens in earlier age. The other is via the direct regulation of bone cells in the process of bone remodelling and predominant occurs in mature

age. Further investigation of the $P2Y_{13}$ receptor's role in phosphate homeostasis may advance our knowledge of phosphate homeostatic mechanisms and provide potential targets to treat phosphate metabolism related bone defects including both hypo and hyperphosphatemia.

References:

1. Burnstock, G. (2002) Purinergic signaling and vascular cell proliferation and death. Arterioscler Thromb Vasc Biol **22**, 364-373
2. Burnstock, G., and Ulrich, H. (2011) Purinergic signaling in embryonic and stem cell development. Cell Mol Life Sci **68**, 1369-1394
3. Hatori, M., Teixeira, C. C., Debolt, K., Pacifici, M., and Shapiro, I. M. (1995) Adenine nucleotide metabolism by chondrocytes in vitro: role of ATP in chondrocyte maturation and matrix mineralization. J Cell Physiol **165**, 468-474
4. Hung, C. T., Allen, F. D., Mansfield, K. D., and Shapiro, I. M. (1997) Extracellular ATP modulates [Ca2+]i in retinoic acid-treated embryonic chondrocytes. Am J Physiol **272**, C1611-1617
5. Kaplan, A. D., Kilkenny, D. M., Hill, D. J., and Dixon, S. J. (1996) Extracellular nucleotides act through P2U purinoceptors to elevate [Ca2+]i and enhance basic fibroblast growth factor-induced proliferation in sheep chondrocytes. Endocrinology **137**, 4757-4766
6. Caswell, A. M., Leong, W. S., and Russell, R. G. (1991) Evidence for the presence of P2-purinoceptors at the surface of human articular chondrocytes in monolayer culture. Biochimica et biophysica acta **1074**, 151-158
7. Koolpe, M., Pearson, D., and Benton, H. P. (1999) Expression of both P1 and P2 purine receptor genes by human articular chondrocytes and profile of ligand-mediated prostaglandin E2 release. Arthritis and rheumatism **42**, 258-267
8. Knight, M. M., McGlashan, S. R., Garcia, M., Jensen, C. G., and Poole, C. A. (2009) Articular chondrocytes express connexin 43 hemichannels and P2 receptors - a putative mechanoreceptor complex involving the primary cilium? J Anat **214**, 275-283
9. Communi, D., Gonzalez, N. S., Detheux, M., Brezillon, S., Lannoy, V., Parmentier, M., and Boeynaems, J. M. (2001) Identification of a novel human ADP receptor coupled to G(i). J Biol Chem **276**, 41479-41485
10. Abbracchio, M. P., Boeynaems, J. M., Barnard, E. A., Boyer, J. L., Kennedy, C., Miras-Portugal, M. T., King, B. F., Gachet, C., Jacobson, K. A., Weisman, G. A., and Burnstock, G. (2003) Characterization of the UDP-glucose receptor (re-named here the P2Y14 receptor) adds diversity to the P2Y receptor family. Trends Pharmacol Sci **24**, 52-55
11. Wittenberger, T., Schaller, H. C., and Hellebrand, S. (2001) An expressed sequence tag (EST) data mining strategy succeeding in the discovery of new G-protein coupled receptors. J Mol Biol **307**, 799-813
12. Zhang, F. L., Luo, L., Gustafson, E., Palmer, K., Qiao, X., Fan, X., Yang, S., Laz, T. M., Bayne, M., and Monsma, F., Jr. (2002) P2Y(13): identification and characterization of a novel Galphai-coupled ADP receptor from human and mouse. J Pharmacol Exp Ther **301**, 705-713

13. Fumagalli, M., Trincavelli, L., Lecca, D., Martini, C., Ciana, P., and Abbracchio, M. P. (2004) Cloning, pharmacological characterisation and distribution of the rat G-protein-coupled P2Y(13) receptor. Biochem Pharmacol **68**, 113-124
14. Csolle, C., Heinrich, A., Kittel, A., and Sperlagh, B. (2008) P2Y receptor mediated inhibitory modulation of noradrenaline release in response to electrical field stimulation and ischemic conditions in superfused rat hippocampus slices. J Neurochem **106**, 347-360
15. Heinrich, A., Kittel, A., Csolle, C., Sylvester Vizi, E., and Sperlagh, B. (2008) Modulation of neurotransmitter release by P2X and P2Y receptors in the rat spinal cord. Neuropharmacology **54**, 375-386
16. Queiroz, G., Talaia, C., and Goncalves, J. (2003) ATP modulates noradrenaline release by activation of inhibitory P2Y receptors and facilitatory P2X receptors in the rat vas deferens. J Pharmacol Exp Ther **307**, 809-815
17. Grimm, I., Messemer, N., Stanke, M., Gachet, C., and Zimmermann, H. (2009) Coordinate pathways for nucleotide and EGF signaling in cultured adult neural progenitor cells. J Cell Sci **122**, 2524-2533
18. Fabre, A. C., Malaval, C., Ben Addi, A., Verdier, C., Pons, V., Serhan, N., Lichtenstein, L., Combes, G., Huby, T., Briand, F., Collet, X., Nijstad, N., Tietge, U. J., Robaye, B., Perret, B., Boeynaems, J. M., and Martinez, L. O. (2010) P2Y13 receptor is critical for reverse cholesterol transport. Hepatology **52**, 1477-1483
19. Wang, N., Robaye, B., Agrawal, A., Skerry, T. M., Boeynaems, J. M., and Gartland, A. (2012) Reduced bone turnover in mice lacking the P2Y(13) receptor of ADP. Mol Endocrinol **26**, 142-152
20. Biver, G., Wang, N., Gartland, A., Orriss, I., Arnett, T. R., Boeynaems, J. M., and Robaye, B. (2013) Role of the P2Y13 receptor in the differentiation of bone marrow stromal cells into osteoblasts and adipocytes. Stem Cells
21. Wang, N., Rumney, R. M., Yang, L., Robaye, B., Boeynaems, J. M., Skerry, T. M., and Gartland, A. (2013) The P2Y13 receptor regulates extracellular ATP metabolism and the osteogenic response to mechanical loading. J Bone Miner Res **28**, 1446-1456
22. Perwad, F., Azam, N., Zhang, M. Y., Yamashita, T., Tenenhouse, H. S., and Portale, A. A. (2005) Dietary and serum phosphorus regulate fibroblast growth factor 23 expression and 1,25-dihydroxyvitamin D metabolism in mice. Endocrinology **146**, 5358-5364
23. Ferrari, S. L., Bonjour, J. P., and Rizzoli, R. (2005) Fibroblast growth factor-23 relationship to dietary phosphate and renal phosphate handling in healthy young men. J Clin Endocrinol Metab **90**, 1519-1524
24. Burnett, S. M., Gunawardene, S. C., Bringhurst, F. R., Juppner, H., Lee, H., and Finkelstein, J. S. (2006) Regulation of C-terminal and intact FGF-23 by dietary phosphate in men and women. J Bone Miner Res **21**, 1187-1196
25. Juppner, H., Wolf, M., and Salusky, I. B. (2010) FGF-23: More than a regulator of renal phosphate handling? J Bone Miner Res **25**, 2091-2097
26. Shimada, T., Kakitani, M., Yamazaki, Y., Hasegawa, H., Takeuchi, Y., Fujita, T., Fukumoto, S., Tomizuka, K., and Yamashita, T. (2004) Targeted ablation of Fgf23 demonstrates an essential physiological role of FGF23 in phosphate and vitamin D metabolism. J Clin Invest **113**, 561-568
27. Mackenzie, N. C., Zhu, D., Milne, E. M., van 't Hof, R., Martin, A., Quarles, D. L., Millan, J. L., Farquharson, C., and MacRae, V. E. (2012) Altered bone development and an increase in FGF-23 expression in Enpp1(-/-) mice. PLoS One **7**, e32177

28. Yoshiko, Y., Wang, H., Minamizaki, T., Ijuin, C., Yamamoto, R., Suemune, S., Kozai, K., Tanne, K., Aubin, J. E., and Maeda, N. (2007) Mineralized tissue cells are a principal source of FGF23. Bone **40**, 1565-1573
29. Parfitt, A. M., Drezner, M. K., Glorieux, F. H., Kanis, J. A., Malluche, H., Meunier, P. J., Ott, S. M., and Recker, R. R. (1987) Bone histomorphometry: standardization of nomenclature, symbols, and units. Report of the ASBMR Histomorphometry Nomenclature Committee. J Bone Miner Res **2**, 595-610
30. Marionneau, C., Couette, B., Liu, J., Li, H., Mangoni, M. E., Nargeot, J., Lei, M., Escande, D., and Demolombe, S. (2005) Specific pattern of ionic channel gene expression associated with pacemaker activity in the mouse heart. J Physiol **562**, 223-234
31. Hildebrand, T., and Ruegsegger, P. (1997) Quantification of Bone Microarchitecture with the Structure Model Index. Comput Methods Biomech Biomed Engin **1**, 15-23
32. Sondergaard, M., Dagnaes-Hansen, F., Flyvbjerg, A., and Jensen, T. G. (2003) Normalization of growth in hypophysectomized mice using hydrodynamic transfer of the human growth hormone gene. Am J Physiol Endocrinol Metab **285**, E427-432
33. Livak, K. J., and Schmittgen, T. D. (2001) Analysis of relative gene expression data using real-time quantitative PCR and the 2(-Delta Delta C(T)) Method. Methods **25**, 402-408
34. Pinter, O., Beda, Z., Csaba, Z., and Csaba, I. (2007) Differences in the onset of puberty in selected inbred mouse strains. Endocrine Abstracts **14**, P617
35. Rhees, B. K., and Atchley, W. R. (2000) Body weight and tail length divergence in mice selected for rate of development. J Exp Zool **288**, 151-164
36. van der Eerden, B. C., Karperien, M., and Wit, J. M. (2003) Systemic and local regulation of the growth plate. Endocr Rev **24**, 782-801
37. Razzaque, M. S., Sitara, D., Taguchi, T., St-Arnaud, R., and Lanske, B. (2006) Premature aging-like phenotype in fibroblast growth factor 23 null mice is a vitamin D-mediated process. FASEB J **20**, 720-722
38. Lanske, B., and Razzaque, M. S. (2007) Mineral metabolism and aging: the fibroblast growth factor 23 enigma. Curr Opin Nephrol Hypertens **16**, 311-318
39. Shalhoub, V., Ward, S. C., Sun, B., Stevens, J., Renshaw, L., Hawkins, N., and Richards, W. G. (2011) Fibroblast growth factor 23 (FGF23) and alpha-klotho stimulate osteoblastic MC3T3.E1 cell proliferation and inhibit mineralization. Calcif Tissue Int **89**, 140-150
40. Wang, H., Yoshiko, Y., Yamamoto, R., Minamizaki, T., Kozai, K., Tanne, K., Aubin, J. E., and Maeda, N. (2008) Overexpression of fibroblast growth factor 23 suppresses osteoblast differentiation and matrix mineralization in vitro. J Bone Miner Res **23**, 939-948
41. Beck, G. R., Jr. (2003) Inorganic phosphate as a signaling molecule in osteoblast differentiation. J Cell Biochem **90**, 234-243
42. Shimada, T., Mizutani, S., Muto, T., Yoneya, T., Hino, R., Takeda, S., Takeuchi, Y., Fujita, T., Fukumoto, S., and Yamashita, T. (2001) Cloning and characterization of FGF23 as a causative factor of tumor-induced osteomalacia. Proc Natl Acad Sci U S A **98**, 6500-6505
43. Ben-Dov, I. Z., Galitzer, H., Lavi-Moshayoff, V., Goetz, R., Kuro-o, M., Mohammadi, M., Sirkis, R., Naveh-Many, T., and Silver, J. (2007) The parathyroid is a target organ for FGF23 in rats. J Clin Invest **117**, 4003-4008
44. Krajisnik, T., Bjorklund, P., Marsell, R., Ljunggren, O., Akerstrom, G., Jonsson, K. B., Westin, G., and Larsson, T. E. (2007) Fibroblast growth factor-23 regulates

parathyroid hormone and 1alpha-hydroxylase expression in cultured bovine parathyroid cells. J Endocrinol **195**, 125-131
45. Boyan, B. D., Sylvia, V. L., Dean, D. D., Del Toro, F., and Schwartz, Z. (2002) Differential Regulation of Growth Plate Chondrocytes by 1α,25-$(OH)_2D_3$ and 24R,25-$(OH)_2D_3$ Involves Cell-maturation-specific Membrane-receptor-activated Phospholipid Metabolism. Crit Rev Oral Biol Med **13**, 143-154
46. Stubbs, J. R., He, N., Idiculla, A., Gillihan, R., Liu, S., David, V., Hong, Y., and Quarles, L. D. (2012) Longitudinal evaluation of FGF23 changes and mineral metabolism abnormalities in a mouse model of chronic kidney disease. J Bone Miner Res **27**, 38-46
47. Moe, S., Drueke, T., Cunningham, J., Goodman, W., Martin, K., Olgaard, K., Ott, S., Sprague, S., Lameire, N., and Eknoyan, G. (2006) Definition, evaluation, and classification of renal osteodystrophy: a position statement from Kidney Disease: Improving Global Outcomes (KDIGO). Kidney Int **69**, 1945-1953
48. Wang, G., Woods, A., Sabari, S., Pagnotta, L., Stanton, L. A., and Beier, F. (2004) RhoA/ROCK signaling suppresses hypertrophic chondrocyte differentiation. J Biol Chem **279**, 13205-13214
49. Saito, H., Maeda, A., Ohtomo, S., Hirata, M., Kusano, K., Kato, S., Ogata, E., Segawa, H., Miyamoto, K., and Fukushima, N. (2005) Circulating FGF-23 is regulated by 1alpha,25-dihydroxyvitamin D3 and phosphorus in vivo. J Biol Chem **280**, 2543-2549
50. Farrow, E. G., Summers, L. J., Schiavi, S. C., McCormick, J. A., Ellison, D. H., and White, K. E. (2010) Altered renal FGF23-mediated activity involving MAPK and Wnt: effects of the Hyp mutation. J Endocrinol **207**, 67-75
51. Bacic, D., Schulz, N., Biber, J., Kaissling, B., Murer, H., and Wagner, C. A. (2003) Involvement of the MAPK-kinase pathway in the PTH-mediated regulation of the proximal tubule type IIa Na+/Pi cotransporter in mouse kidney. Pflugers Arch **446**, 52-60
52. Segawa, H., Kaneko, I., Takahashi, A., Kuwahata, M., Ito, M., Ohkido, I., Tatsumi, S., and Miyamoto, K. (2002) Growth-related renal type II Na/Pi cotransporter. J Biol Chem **277**, 19665-19672
53. Unwin, R. J., Bailey, M. A., and Burnstock, G. (2003) Purinergic signaling along the renal tubule: the current state of play. News Physiol Sci **18**, 237-241
54. Vallon, V. (2008) P2 receptors in the regulation of renal transport mechanisms. Am J Physiol Renal Physiol **294**, F10-27
55. Praetorius, H. A., and Leipziger, J. (2010) Intrarenal purinergic signaling in the control of renal tubular transport. Annu Rev Physiol **72**, 377-393
56. Inscho, E. W. (2009) Purinoceptor regulation of renal tubular transport is coming of age. Am J Physiol Renal Physiol **297**, F1166-1167
57. Bailey, M. A., and Shirley, D. G. (2009) Effects of extracellular nucleotides on renal tubular solute transport. Purinergic Signal **5**, 473-480
58. Biber, J., Hernando, N., Forster, I., and Murer, H. (2009) Regulation of phosphate transport in proximal tubules. Pflugers Arch **458**, 39-52
59. Wang, L., Olivecrona, G., Gotberg, M., Olsson, M. L., Winzell, M. S., and Erlinge, D. (2005) ADP acting on P2Y13 receptors is a negative feedback pathway for ATP release from human red blood cells. Circ Res **96**, 189-196

Acknowledgements. Funding Source: European Commission under the 7th Framework Programme (proposal #202231) performed as a collaborative project among the members of the ATPBone Consortium (Copenhagen University, University College London, University of Maastricht, University of Ferrara, University of Liverpool, University of Sheffield, and Université Libre de Bruxelles), and is a sub study under the main study "Fighting osteoporosis by blocking nucleotides: purinergic signalling in bone formation and homeostasis".

Disclosure summary: All authors have nothing to disclose.

Table 1. Age related parameters of tibial trabecular bone using μCT analysis.

		2 Weeks	Mean percent difference	p	**4 Weeks**	Mean percent difference	p	**10 Weeks**	Mean percent difference	p	**16 Weeks**	Mean percent difference	p
BMD (g/cm^3)	**WT**	0.97 ± 0.006	↑0.8%		0.98 ± 0.009	↑3.0%	a	1.04 ± 0.009	↑3.3%	a	1.15 ± 0.007	↑0.2%	
	KO	0.98 ± 0.011			1.01 ± 0.006			1.07 ± 0.009			1.15 ± 0.010		
BV/TV	**WT**	3.58 ± 0.238	↓2.3%		5.14 ± 0.104	↑13.5%	a	9.77 ± 0.317	↓14.4%	a	9.17 ± 0.340	↓37.5%	c
	KO	3.50 ± 0.255			5.83 ± 0.258			8.36 ± 0.412			5.73 ± 0.634		
Tb.Th (mm)	**WT**	0.0246 ± 0.0002	↑2.4%	a	0.028 ± 0.0003	↑6.7%	a	0.038 ± 0.0006	↑9.4%	b	0.048 ± 0.0006	↑0.8%	
	KO	0.0253 ± 0.0001			0.030 ± 0.0006			0.041 ± 0.0006			0.049 ± 0.0018		
Tb.N (1/mm)	**WT**	1.45 ± 0.093	↓4.4%		1.83 ± 0.036	↑6.5%		2.61 ± 0.112	↓21.8%	b	1.89 ± 0.054	↓37.8%	c
	KO	1.39 ± 0.105			1.95 ± 0.098			2.04 ± 0.109			1.18 ± 0.132		
Tb.Pf (1/mm)	**WT**	56.55 ± 1.628	↓0.05%		41.77 ± 0.925	↓5.7%		30.56 ± 0.551	↑3.5%		26.18 ± 0.992	↑21.5%	b
	KO	56.52 ± 0.969			39.39 ± 1.456			31.63 ± 1.150			31.81 ± 1.607		
Tb.Sp (mm)	**WT**	0.30 ± 0.009	↑4.1%		0.24 ± 0.010	↓6.2%		0.19 ± 0.005	↑21.9%	c	0.23 ± 0.003	↑43.2%	c
	KO	0.32 ± 0.010			0.23 ± 0.008			0.23 ± 0.009			0.33 ± 0.024		
SMI	**WT**	2.27 ± 0.035	↑1.2%		2.04 ± 0.019	↑1.2%		2.03 ± 0.026	↑6.4%	a	2.13 ± 0.031	↑13.0%	b
	KO	2.30 ± 0.018			2.06 ± 0.040			2.17 ± 0.051			2.41 ± 0.074		
DA	**WT**	4.25 ± 0.386	↓22.9%		3.54 ± 0.241	↑4.1%		2.52 ± 0.067	↓2.5%		2.49 ± 0.078	↓ 22.0%	c
	KO	3.27 ± 0.354			3.39 ± 0.306			2.45 ± 0.128			1.94 ± 0.051		

Values are mean ± SEM

Mean percent difference = $(KO_{mean} - WT_{mean})/WT_{mean} \times 100$

[a] $p < 0.05$, [b] $p < 0.01$, [c] $p < 0.001$ (unpaired t-test)

List of Figure Legends

Figure 1. Neonatal KO mice have a normal bone phenotype. KO and WT littermate controls were obtained from heterozygous breeding pairs. Neonatal mice were genotyped and euthanized within 24 hours after birth. **(A)** Gross appearance of KO and WT littermates, scale bar = 5.0 mm, and **(B)** body weight comparison, WT n = 14, KO n = 23. Whole skeletons of pup were oversize scanned at the resolution of 17.2µm using the Skyscan 1172 µCT machine and analyzed to obtain **(C)** 3D models of the whole skeleton, scale bar = 5.0 mm, and **(D)** total bone volume fraction (BV/TV). The neonatal pups were also skinned, eviscerated, and stained with alizarin red/alcian blue. After staining, the cartilage and ossified bone were clearly stained as blue and red respectively, which can be seen on the dorsal view of the stained pups, scale bar = 5.0 mm **(E). (G)** The whole length (marked with black line), **(H)** ossified bone length (marked with red line), and **(I)** mid shaft diameter of right femurs were measured using calibrated vernier callipers on the stained right hind limbs, scale bar = 2.0 mm **(F).** All values are mean ± SEM, n = 8 unless specified (unpaired t-test).

Figure 2. Trabecular bone changes with age in KO mice. Right tibiae were isolated from both KO and WT mice at age of 2 weeks, 4 weeks, 10 weeks, and 16 weeks. Proximal ends of tibiae were scanned at the resolution of 4.3µm using the Skyscan 1172 µCT machine. Using the Skyscan CTan and CTvol software, **(A)** 3D models of trabecular region were built to show the trabecular architecture changes with age, scale bar = 0.5 mm, and **(B)** trabecular bone volume fraction (BV/TV) and **(C)** trabecular number (Tb.N) were calculated. All values are mean ± SEM, n = 6-8. ^{a} $p<0.05$, ^{b} $p<0.01$, ^{c} $p<0.001$ (unpaired t-test).

Figure 3. Histomorphometry analysis showed age dependent changes in bone cells in KO mice. Left tibiae were obtained from 4 and 16 weeks old mice. Sections were prepared and TRAP stained. A 3-mm length of endocortical surface 0.25mm away from the growth plate was viewed and quantified on a DMRB microscope using the Osteomeasure bone histomorphometry software. **(A)** Black arrow heads indicated cobble stone like osteoblasts with large nucleus and **(B)** TRAP positive osteoclasts on endocortical surface, scale bar = 50 µm. **(C)** N.Ob/B.Pm, **(D)** Ob.Pm/B.Pm, **(E)** N.Oc/B.Pm and **(F)** Oc.Pm/B.Pm were then evaluated. All values are mean ± SEM, n = 6, ^{a} $p<0.05$, ^{b} $p<0.01$, ^{c} $p<0.001$ (unpaired t-test).

Figure 4. Bone length and growth plate structural alteration with age in KO mice. (A) The tibial lengths of different aged mice (2 weeks, 4 weeks, 10 weeks, and 16 weeks) were measured from the lowest point of the distal end to the highest point of the proximal end using calibrated vernier callipers. **(B)** The lengths of mice tail were also measured at 4 weeks, 10 weeks, and 16 weeks of age, using calibrated vernier callipers. **(C)** Left tibiae of mice at 4, 10 and 16 weeks of age were sectioned and H&E stained PZ = proliferation zone, scale bar = 100μm. The width of each section of growth plate was quantified including **(D)** the measurement of the growth plate total width (including resting, proliferation, and hypertrophic zones) and **(E)** the measurement on proliferation zone only. All values are mean ± SEM, n = 6 – 8, ^{b} $p<0.01$, ^{c} $p<0.001$ (unpaired t-test).

Figure 5. Serum biochemical marker variation in young and old KO mice. (A) Phosphorus, **(B)** calcium, and **(D)** ALP were measured using Modular Analytics analyser in serum samples of 4 weeks and 20 weeks old mice, n = 7~8**. (C)** Serum FGF-23 level was measured by ELISA in serum samples taken mice at 4 weeks and 16 weeks of age, n = 5. **(E)** Serum 25-0H vitamin D3 was measured using an immunometric method with chemoluminescence, n = 3~4. All values are mean ± SEM, ^{a} $p<0.05$, ^{c} $p<0.001$ (unpaired t-test).

FIG. 1

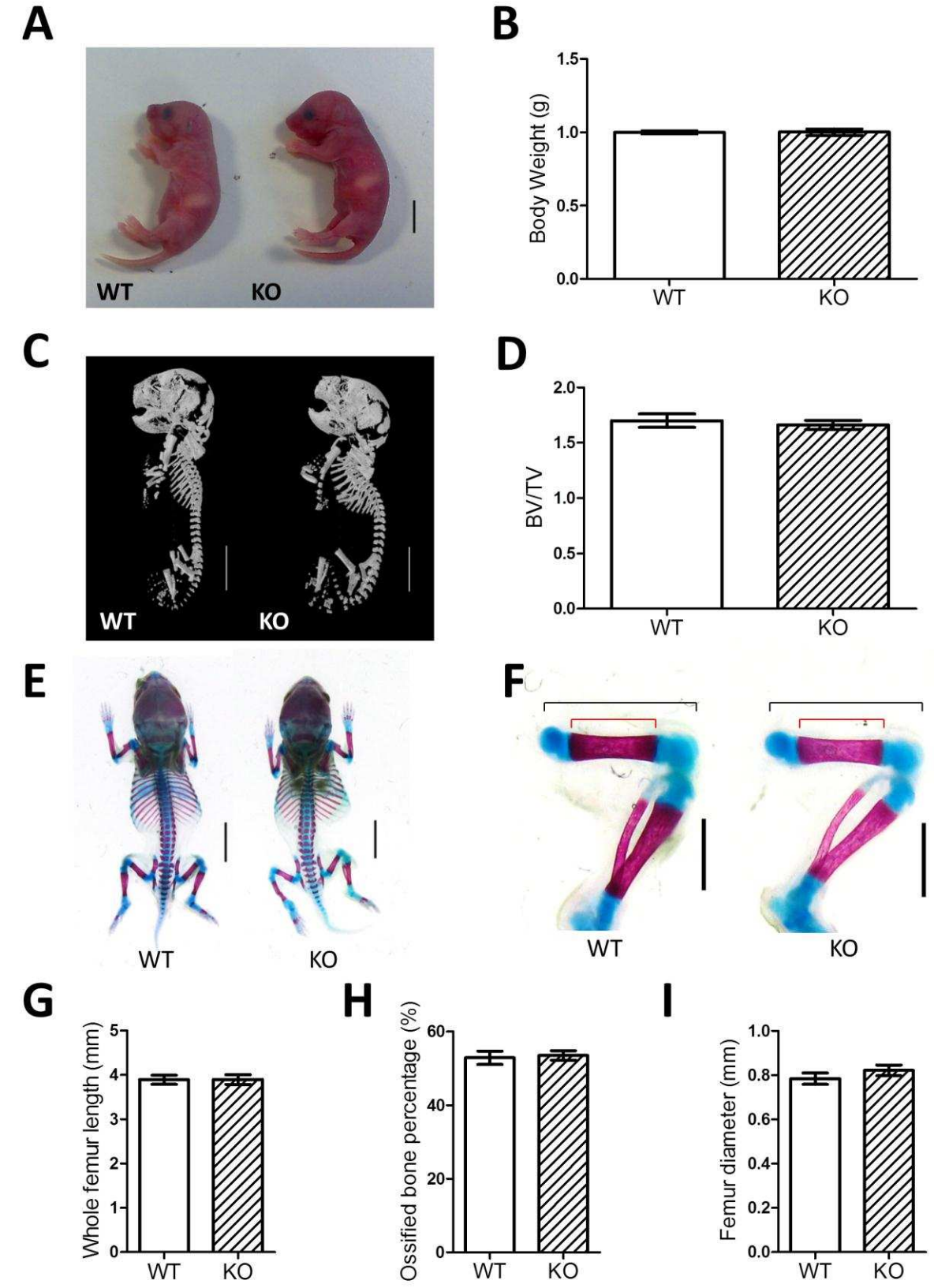
A
WT
KO
B
Body Weight (g)
1.5
1.0
0.5
0.0
WT
KO
C
WT
KO
D
BV/TV
2.0
1.5
1.0
0.5
0.0
WT
KO
E
WT
KO
F
WT
KO
G
Whole femur length (mm)
5
4
3
2
1
0
WT
KO
H
Ossified bone percentage (%)
60
40
20
0
WT
KO
I
Femur diameter (mm)
1.0
0.8
0.6
0.4
0.2
0.0
WT
KO

FIG. 2

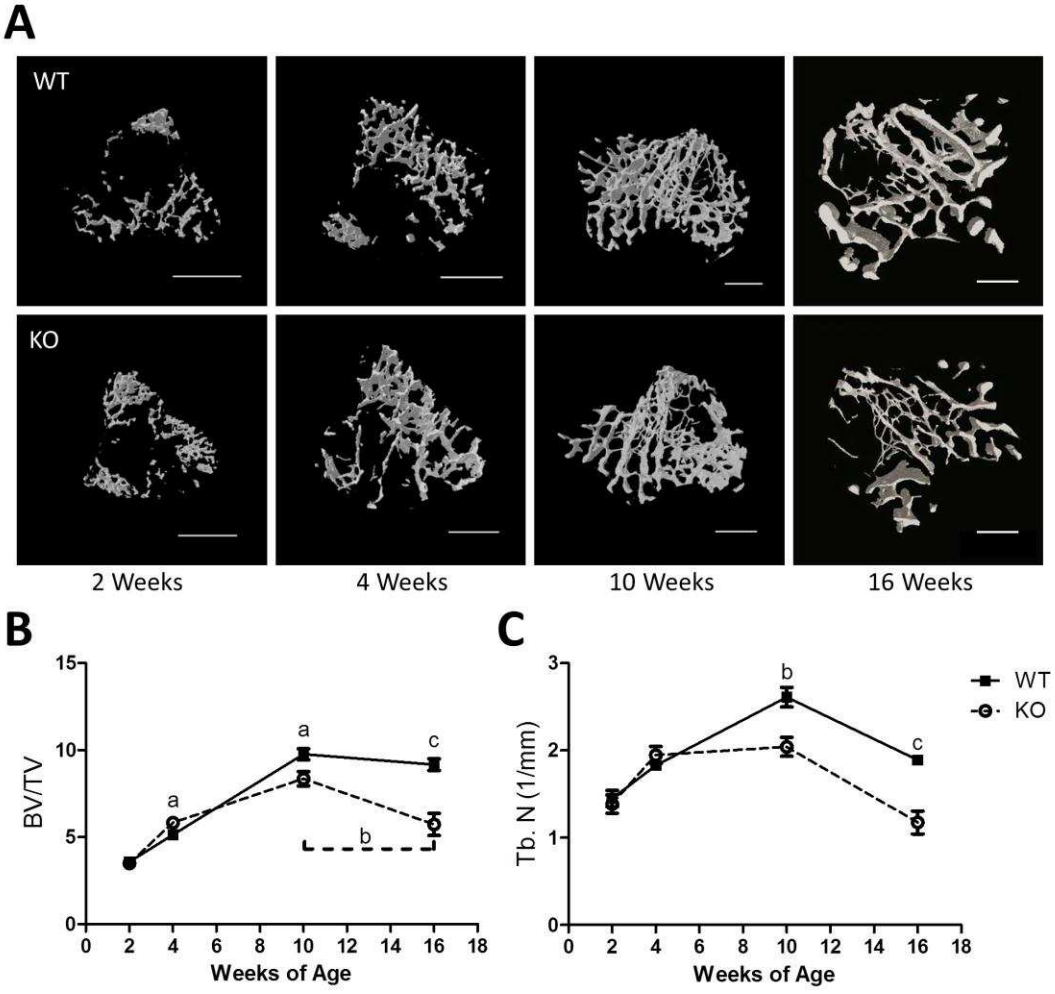
A
WT
KO
2 Weeks
4 Weeks
10 Weeks
16 Weeks
B
BV/TV
Weeks of Age
C
Tb. N (1/mm)
Weeks of Age
WT
KO

FIG. 3

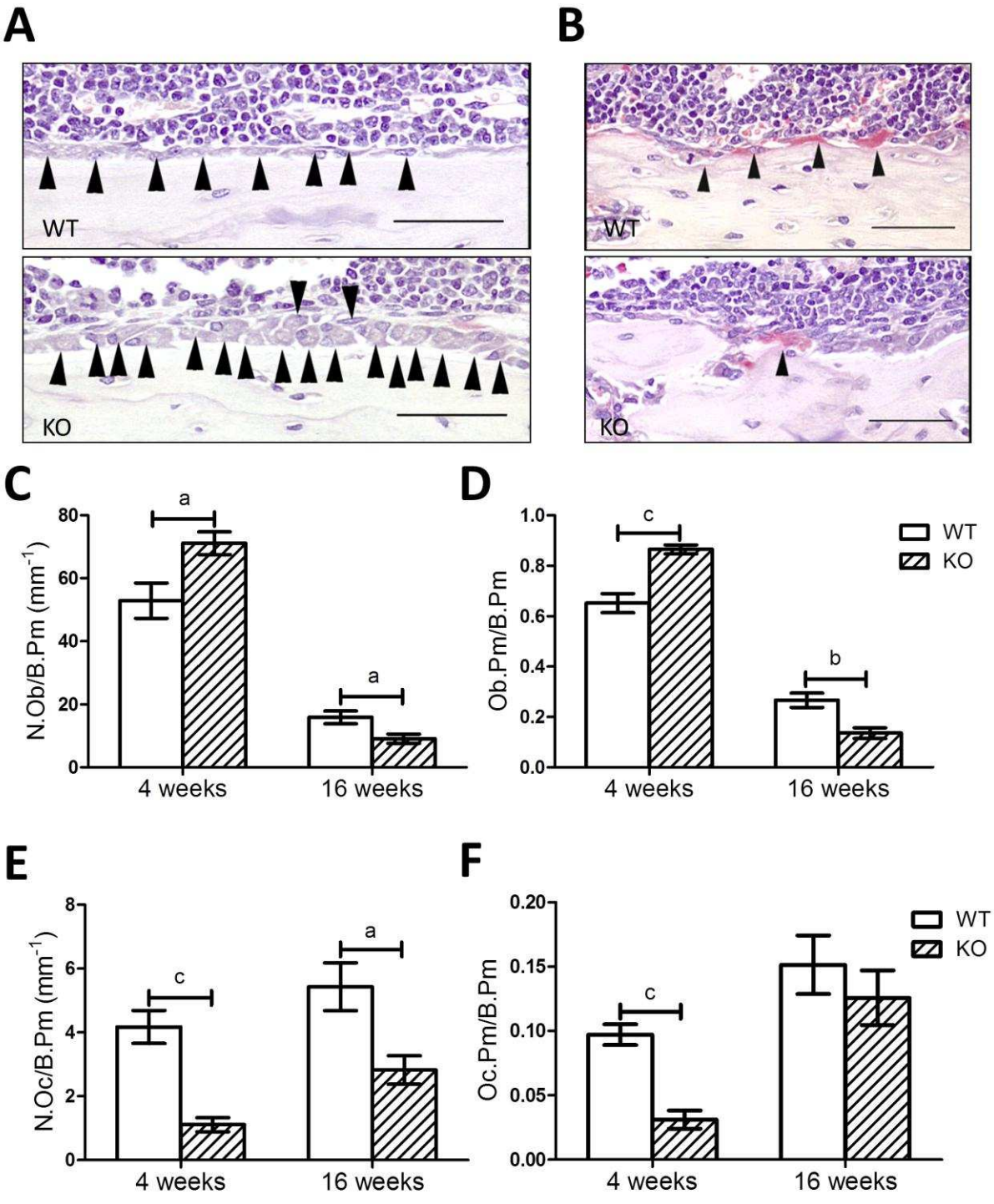
A
B
WT
KO
WT
KO
C
N.Ob/B.Pm (mm-1)
80
60
40
20
0
a
a
4 weeks
16 weeks
D
Ob.Pm/B.Pm
1.0
0.8
0.6
0.4
0.2
0.0
c
b
WT
KO
4 weeks
16 weeks
E
N.Oc/B.Pm (mm-1)
8
6
4
2
0
c
a
4 weeks
16 weeks
F
Oc.Pm/B.Pm
0.20
0.15
0.10
0.05
0.00
c
WT
KO
4 weeks
16 weeks

FIG. 4

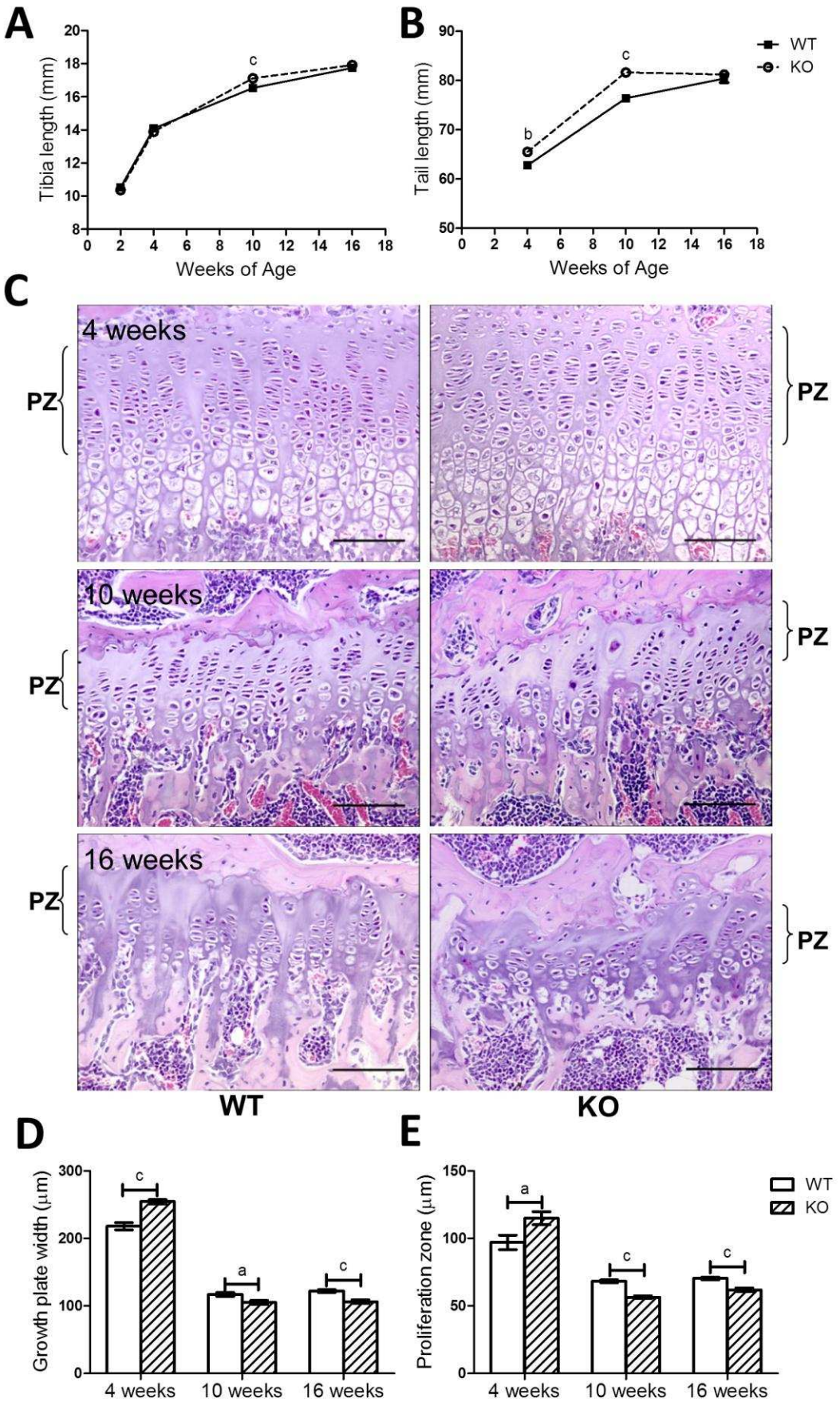
A
Tibia length (mm)
Weeks of Age
c
B
Tail length (mm)
Weeks of Age
b
c
WT
KO
C
4 weeks
10 weeks
16 weeks
PZ
WT
KO
D
Growth plate width (μm)
c
a
c
4 weeks
10 weeks
16 weeks
E
Proliferation zone (μm)
a
c
c
WT
KO
4 weeks
10 weeks
16 weeks

FIG. 5

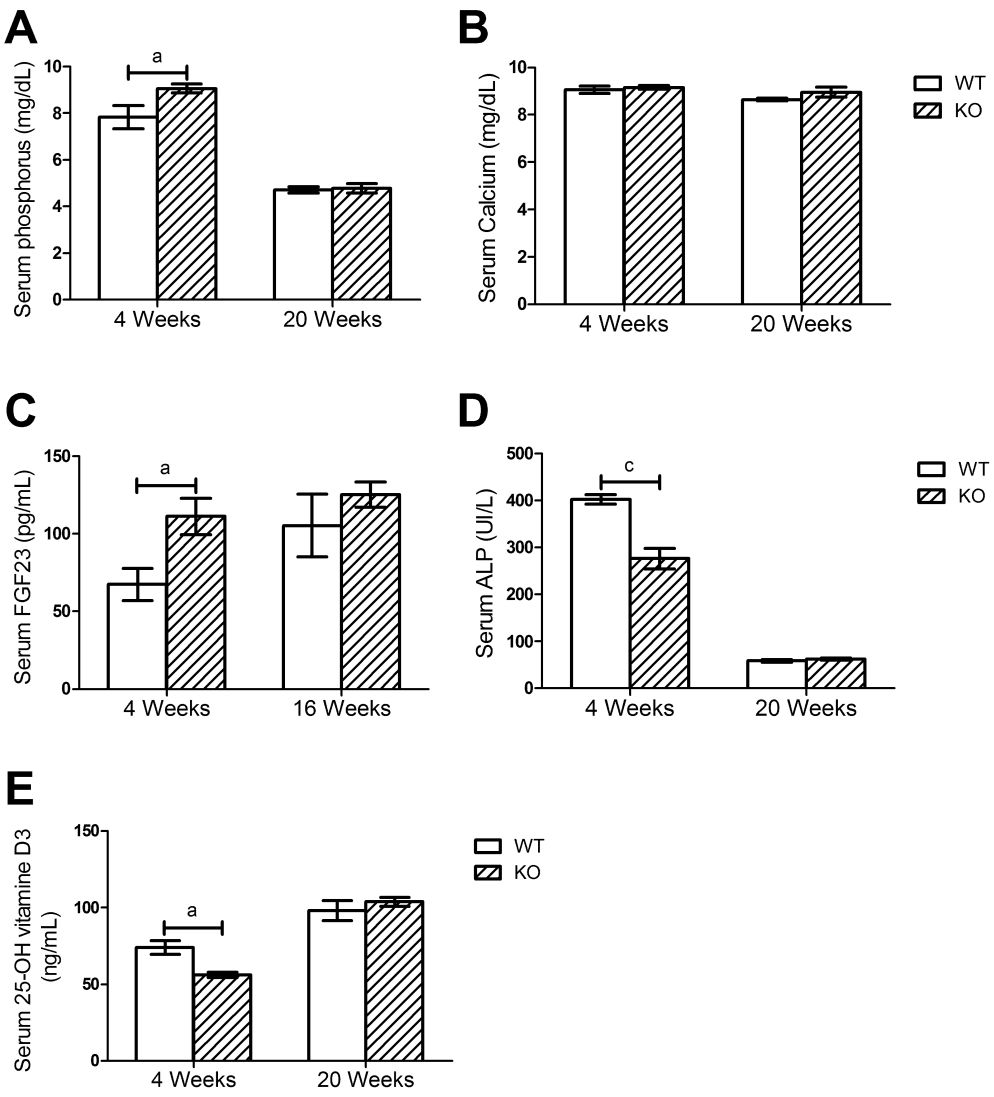
A
Serum phosphorus (mg/dL)
a
4 Weeks
20 Weeks
B
Serum Calcium (mg/dL)
WT
KO
4 Weeks
20 Weeks
C
Serum FGF23 (pg/mL)
a
4 Weeks
16 Weeks
D
Serum ALP (UI/L)
c
WT
KO
4 Weeks
20 Weeks
E
Serum 25-OH vitamine D3 (ng/mL)
a
WT
KO
4 Weeks
20 Weeks